



Overlay-independent comparisons of X-ray structures reveal small, systematic conformational changes in liganded acetylcholinesterase

JACQUELINE ROHRER¹
MORGANA SIDHOM¹
JINGTING HAN¹
ZORAN RADIĆ*

Skaggs School of Pharmacy and Pharmaceutical
Sciences, University of California at San Diego
La Jolla, CA 92093-0650

¹ Contributed equally to the study.

***Correspondence:**

Zoran Radić
zradic@ucsd.edu

Received December 17, 2016.
Revised December 29, 2016.
Accepted December 29, 2016.

Abstract

Background and Purpose: Comparisons of macromolecular 3D structures by minimizing corresponding atom RMSDs can by virtue of averaging, hide small unexpected deviations caused by ligand binding or site-directed mutagenesis. We developed an overlay-independent comparison approach and used it to compare selected, PDB structures of acetylcholinesterase (AChE; EC 3.1.1.7) in the apo state, in complexes with reversible ligands, in covalent conjugates or upon AChE mutagenesis.

Methods: The active serine alpha carbon of the AChE monomer was used as a frame of reference for each of the structures and distances calculated to remaining alpha carbons of the monomer backbone. Differences in distances at corresponding backbone positions from pairwise comparisons with apo-AChE structures were taken as a measure of changes in tertiary structures of liganded or mutant AChE monomers.

Results: This analysis revealed small, yet significant backbone shifts in monomeric tertiary structures of AChEs. While reversible complexes with neurotoxin Fas2 showed global expansion of AChE monomer backbones, covalent conjugates at the active serine and high affinity reversible inhibitor hupA complexes revealed backbone compression towards the active serine. In some of AChE homodimers 0.6 – 1Å shifts of monomer backbone affected crystallographic quaternary structures by causing significant, up to seven degree tilts in monomers, relative to angles measured in the apo-AChE.

Conclusions: Small but systematic differences detected in tertiary structures of liganded or mutagenized AChEs appear consistent with larger magnitude alterations of several AChE homodimer quaternary structures. Those observations validate our overlay-independent approach for detecting small, yet significant, tertiary backbone shifts in macromolecular 3D structures.

INTRODUCTION

Insights into structural properties of acetylcholinesterase (AChE; EC 3.1.1.7), one of essential proteins of cholinergic neurotransmission in vertebrates, were largely achieved by resolutions of its primary (1), secondary (2) and tertiary, 3D (3) structures for the protein found in electric organs of the fish *Torpedo californica*. To date, around 200 X-ray structures of AChEs from various species, mainly fish, mouse and human, but also insect and snake AChEs have been deposited to PDB in the apo state, in complexes with variety of structurally diverse reversible ligands or as small molecule covalent conjugates at the active serine. In

spite of sufficiently high resolutions (of $\sim 2 - 2.5 \text{ \AA}$), vast majority of those 3D structures, in particular those from fish, mouse and human, share very high degree of similarity in their alpha carbon backbone fold, and associated overlay RMSD values are well below 1 \AA (4). This similarity extends even to complexes with active center ligands larger than the size of the AChE active center entry, such as huperzine A (hupA) or galanthamine where transient openings of the AChE active center gorge seem necessary for complexes to form, yet no 3D structure in the open state has ever been observed for any AChE (5). We used overlay-independent comparisons to find out whether upon examination of a larger number of PDB deposited AChE crystal structures even relatively small but significant deviations of AChE backbone fragments could be identified. Conformational changes in the AChE alpha carbon backbone identified in that way could indicate larger conformational flexibility of AChE in solution. Instead of minimizing RMSD of corresponding alpha carbons in the pair of AChE structures that could easily, by virtue of averaging, hide small deviations in unexpected regions of the structure, we analyzed an independent structural architecture parameter for each of the AChE structures in the pair, such as interatomic distance, and then compared those parameters in a pairwise fashion. We selected the active serine alpha carbon as a frame of reference for each of the structures and calculated its distance to alpha carbons of the AChE backbone. Differences in pairwise comparison of those distances, for a pair of structures were then taken as an indication of a ligand binding associated backbone movement. In this way we identified previously unobserved conformational deviations of the AChE backbone, associated with ligand binding interactions. We furthermore observed that some of those tertiary structure deviations influence subunit ordering in crystallographic AChE homodimers altering the AChE quaternary structure.

We believe that results presented here may be of use in AChE structure/activity considerations, and that some could be experimentally tested and subsequently contribute additional guidance in the AChE structure-based drug discovery and design.

METHODS

All AChE structures analyzed in this study were X-ray diffraction derived and obtained from the Protein Data Bank (PDB), an open resource of macromolecular 3D structures (www.rcsb.org).

Tertiary structure analysis. Structural coordinate files obtained from the PDB were used to extract coordinates of alpha carbons, either by using „egrep” Linux command or by editing.pdb files in the DS Visualizer 4.5 (Biovia, San Diego, CA). Resulting alpha carbon coordinates were imported into a spreadsheet program and used to calcu-

late 3D distances to the active serine using the following equation:

$$\begin{aligned} \text{distance}(p,q) &= \sqrt{(p_1 - q_1)^2 + (p_2 - q_2)^2 + (p_3 - q_3)^2} \quad \text{eq(1)} \\ \Delta \text{ distance}(p) &= \text{distance}^A(p,q) - \text{distance}^B(p,q) \quad \text{eq(2)} \end{aligned}$$

where q_1, q_2 and q_3 are the active serine (q) alpha carbon coordinates and p_1, p_2 and p_3 are coordinates of any other AChE alpha carbon (p). Pairwise differences in corresponding distances between two structures A and B („ Δ distance”) were then calculated for every alpha carbon residue using the eq(2) in the spreadsheet and resulting values graphed as a function of AChE amino acid number (Figure 1C). Furthermore, „ Δ distance” values of each residue were mapped onto a ribbon representation of an alpha carbon AChE backbone using DS Visualizer, as a red-blue color gradient ranging between either -0.6 or -1.0 \AA (deep red) and either 0.6 or 1.0 \AA (deep blue) „ Δ distance” values (Figure 1B). All RMSD calculations included alpha carbons only, were manual sequence alignment based and were all done in DS Visualizer.

Quaternary structure analysis. Relative orientation of monomers in crystallographic AChE dimers were analyzed in two different ways. One approach was to calculate 3D distances (eq(1)) between corresponding alpha carbons of each monomer, in a dimer, and compare those distances pairwise, with corresponding distances determined for the apo form of the AChE. Resulting „ Δ distance” values were graphed as a function of AChE amino acid residue number in the linear sequence and color mapped using red-blue gradient (in the range from -5 \AA to 5 \AA) to a ribbon representation of AChE backbone structure. Red indicates residues of the backbone positioned closer to the equivalent residue of the other monomer of the dimer, while blue indicates parts of the backbone positioned farther then corresponding residues in the apo AChE dimer.

The other approach was to calculate angles between normal vectors for each of three best planes (X-Y, Y-Z and X-Z; Figure 2A) of alpha carbon coordinate datasets between monomers in a dimer (Figure 2B), and then compare those angles to angles found for monomers in the apo AChE dimers. Best plane parameters A, B and C were calculated by regression in Sigmaplot 12.3 (Systat Software, Inc., San Jose, CA) from following equations:

$$\text{for X-Y plane } z = C + A^*x + B^*y \quad \text{eq (3)}$$

$$\text{for Y-Z plane } x = C + A^*z + B^*y \quad \text{eq (4)}$$

$$\text{for X-Z plane } y = C + A^*x + B^*z \quad \text{eq (5)}$$

Angles between normal vectors of structural datasets 1 and 2 were calculated using:

$$\text{angle} = \arccos(\frac{\text{abs}(A_1^*A_2 + B_1^*B_2 + C_1^*C_2)}{\sqrt{(A_1^2 + B_1^2 + C_1^2)} * \sqrt{(A_2^2 + B_2^2 + C_2^2)}}) \quad \text{eq (6)}$$

The difference between normal angles for two datasets (two pairs of best planes: 1 vs 2 and 3 vs 4), „ Δ angle” was calculated from:

$$\Delta \text{ angle} = \text{angle}_{1vs2} - \text{angle}_{3vs4} \quad \text{eq(7)}$$

Resulting „ Δ angle” values were then compared between different structures.

RESULTS AND DISCUSSION

The principle of our overlay-independent approach in comparing protein 3D structures is illustrated in the Fig. 1 B and compared to the RMSD overlay approach (Fig 1A). Interaction of the tight binding snake peptide neu-

rotoxin Fas2 to fish AChE was analyzed first. The overall TcAChE backbone conformation in the pM (10^{-12} M) reversible complex with Fas2 did not change appreciably as judged by the low RMSD overlay value of 0.48 Å (Fig 1A). The overlay-independent comparison, however revealed a number of local backbone shifts of up to ~ 1.5 Å in magnitude (Fig 1C). While catalytic triad Ser and Glu, and oxyanion hole (OAH) remained in the same position as in the apo TcAChE, catalytic triad His and both tip of the Ω loop residues and some surface acyl pocket loop (AP) residues moved as much as 1 Å closer to the active serine and the center of the globular AChE molecule as a consequence of the Fas2 binding. (The center of mass in crystallographic AChE monomers is typically 2 – 3 Å

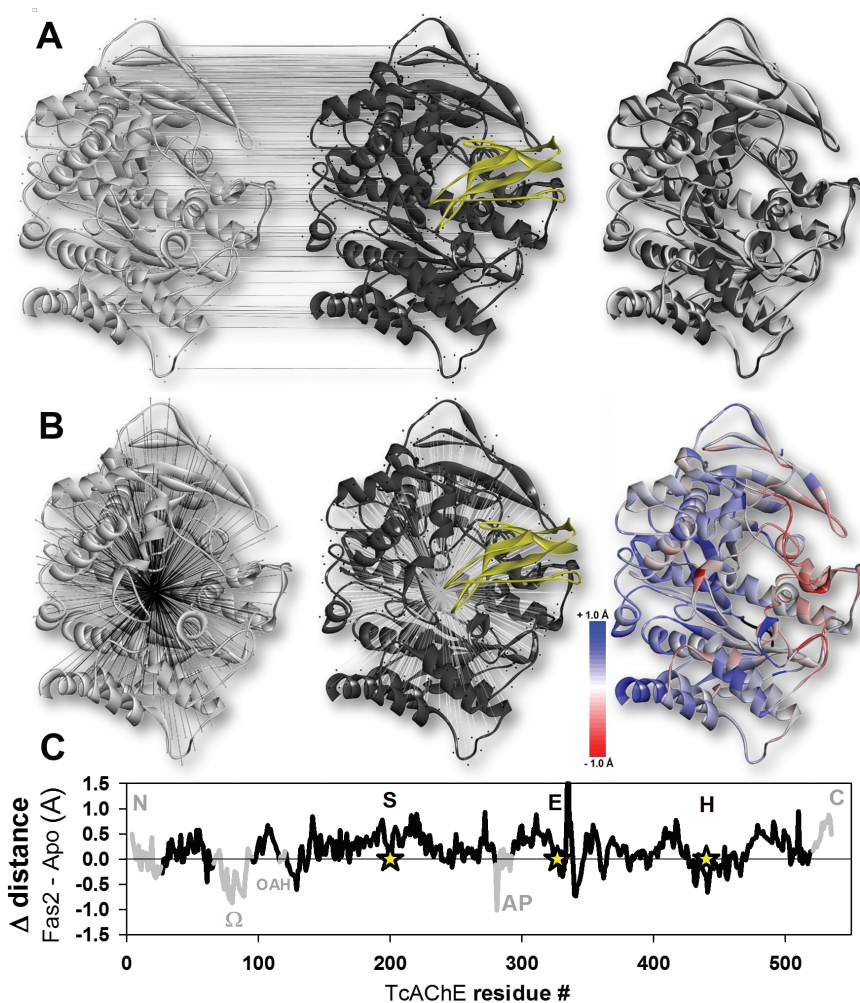


Figure 1. Comparison of tertiary AChE structures. **A)** overlay of apo TcAChE (2ACE; white) and Fas2*TcAChE complex (1FSS; grey, Fas2 ribbon is yellow) based on minimizing RMSD of TcAChE alpha carbons yielding RMSD=0.48 Å. **B)** Overlay-independent comparison of TcAChE backbone conformations based on pairwise calculation of differences in distances (Δ distance) between the active Ser200 alpha carbon and all other alpha carbons, for the apo TcAChE and the complex. Compression of protein backbone fragments towards the active Ser200 (negative Δ distance values, gradient color coded as red ribbon) and its expansion (positive Δ distance values, gradient color coded as blue ribbon) are shown. **C)** Yellow stars in the graph indicate positions of catalytic triad residues (Ser200, Asp 327, His 440). The first 25 N terminal and C terminal residues beyond position 521, consistently showing large flexibility were excluded from subsequent analyses (N and C grey termini). Positions of the Ω loop (residues 67-94) oxyanion hole (OAH, residues 117-119) and the acyl pocket (AP; residues 281-291) are shown in grey as frames of reference in the linear AChE sequence.

close to the active serine alpha carbon). The contractile backbone movement is consistent with previously observed formation of $\sim 2000 \text{ \AA}^2$ large, mainly hydrophobic contact surface area between two molecules (6). Most of alpha carbon shifts (377 out of 527), were however in a direction away from the active serine by an average of 0.31 \AA per residue, while 150 residues moved inwards by an average of 0.23 \AA per residue. Mainly N- and C-terminal domains expanded, while equatorial part of the AChE molecule forming closest direct contact with Fas2 actually contracted, resulting in predominantly blue coloring of the ribbon in the terminal and smaller red domains in the equatorial AChE (Figure 1B).

Similar effect of Fas2 binding was observed in complexes with mouse AChE (mAChE; 1MAH) and human AChE (hAChE; 4EY8) contained in general expansion of the AChE backbone (Figure 3) where 435 mAChE residues expanded by 0.33 \AA and 274 hAChE residues by 0.19 \AA , per residue.

The expansion was particularly consistent in C-terminal alpha helices some of which participate in dimerization domain of AChEs, but also in the $\sim 400 - 420$ alpha helix located immediately below the AChE acyl pocket area, extending towards the catalytic triad (indicated by an arrow in the Figure 3A). The equatorial part of AChEs including Ω loop and parts of the acyl pocket loop predominantly contracted towards the active serine, Ser 203. Consistent alpha backbone motions observed in all three AChE species, in spite of difference in crystallization space groups ($P2_12_12_1$ @ 3 \AA resolution for TcAChE, $P6_322$ @ 3.2 \AA resolution for mAChE and H32 @ 2.6 \AA resolution for hAChE) and associated cell dimensions,

underline value of this overlay-independent structure comparison approach.

Reversible binding of huperzine A (hupA), an inhibitor three order of magnitude less potent than Fas2, with inhibition constants in the nM (10^{-9}M) range, affected alpha backbone in a different manner (Figure 4). HupA binds inside the active center gorge causing systematic compression of all contact areas within AChE, in particular in hAChE where it binds with six-fold higher affinity compared to TcAChE (22 nM vs 130 nM; 7). Dominance of red in color coded AChE ribbons is obvious (Figure 4A) illustrating a „molecular adhesive” effect of bound hupA on AChE. The compression was consistent for the whole hAChE structure (480 residues contracted on average of 0.14 \AA per residue) and not just isolated to Ω loop and acyl pocket loop as observed in Fas2 binding. Some of the surface loops in TcAChE complex deviated slightly outwards, consistent with lower hupA affinity and identity of crystallization conditions ($P3_121$ space group @ 2.3 – 2.5 \AA resolutions for both complexes). It seems that backbone fragments controlling the size of the active center gorge opening, including Ω loop, acyl pocket loop and short helix in the 330 -340 part of the hAChE linear sequence may contribute most to opening motions needed to admit hupA into its binding site.

The effect of covalent inhibitor conjugation with the active serine was analyzed using the only two covalently conjugated hAChE structures currently available in the PDB, conjugates of paraoxon (POX;5HF5; $P3_121$ space group @ 2.15 \AA resolution) and sarin (5FPQ; $P3_121$ space group @ 2.4 \AA resolution). The quick look at the color-coded alpha carbon backbones of two structures reveal

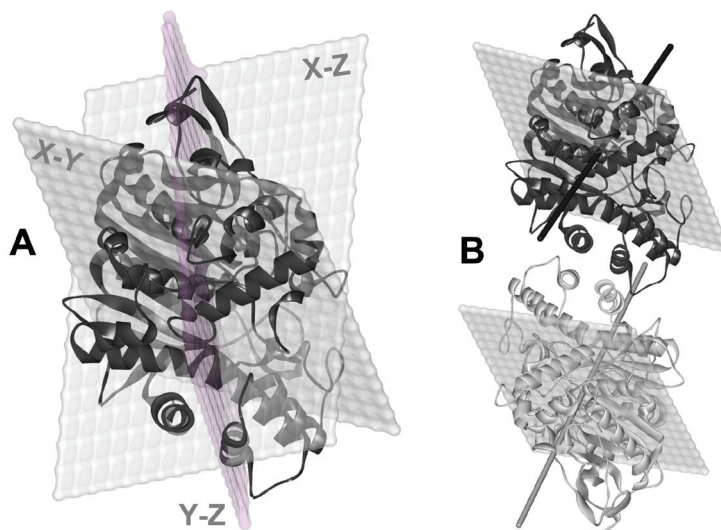


Figure 2. Quaternary structure analysis of relative orientations of monomers in crystallographic homodimers of hAChE (4EY4). **A)** Best planes (X-Y, Y-Z and X-Z) calculated for chain A hAChE, alpha carbon monomer dataset using equations 3 to 5. **B)** Relative positions of normal vectors for X-Y planes calculated for the chain A monomer (dark grey) and chain B monomer (light grey) of the hAChE homodimer. The angle between vectors was 9.6 degrees, calculated from the eq. 6.

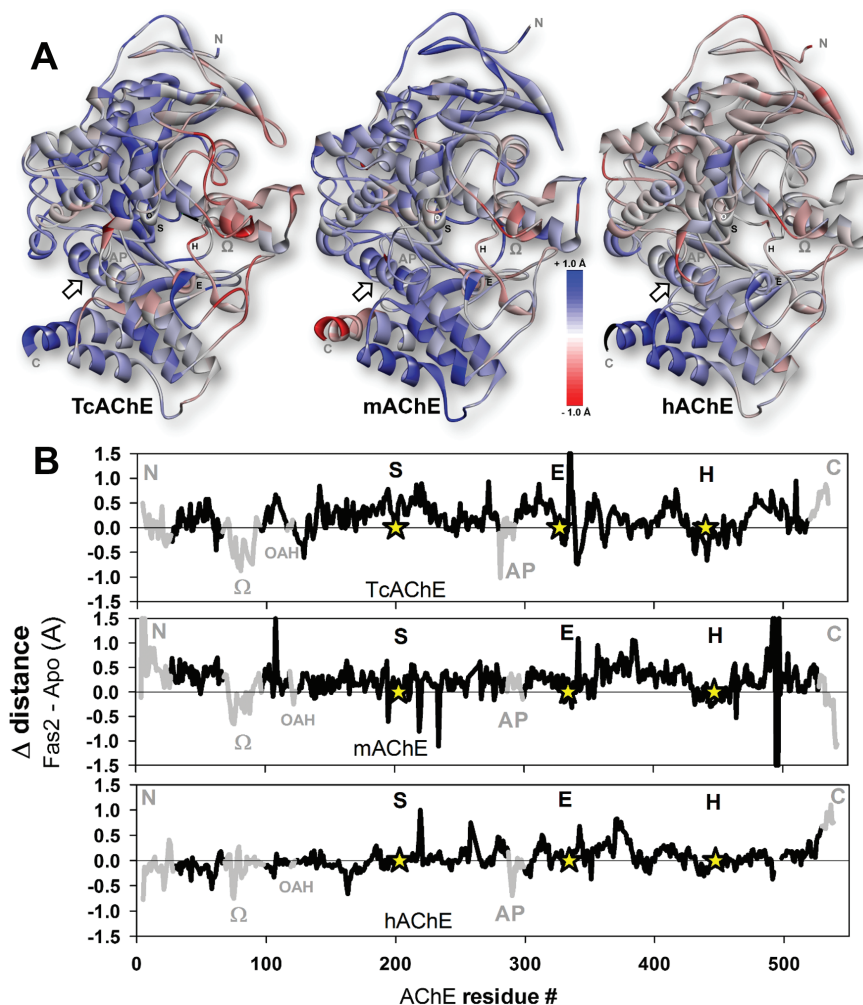


Figure 3. Overlay-independent analysis for the influence of reversible binding of Fas2 on backbone AChE conformations for enzyme from three species TcAChE (1FSS), mAChE (1MAH) and hAChE (4EY8). Fas2 is not shown for clarity. Positions of catalytic triad residues (S,E,H: residues Ser200, Glu327, His440 in TcAChE and Ser203, Glu334, His447 in mAChE and hAChE), oxyanion hole (OAH: residues 117-119 in TcAChE and 120-122 in mAChE and hAChE), Ω loop (residues 67-94 in TcAChE and 69-96 in mAChE and hAChE) and acyl pocket loop (AP: residues 281-291 in TcAChE and 288-298 in mAChE and hAChE) are indicated both in structures (A) and in graphs (B) as described in the Fig 1 legend. Arrow indicates movable helix 410 – 420 (mammalian AChE numbering).

almost complete absence of blue color (Figure 5) and associated positive „ Δ distance” values, indicating global contraction of AChE backbones upon covalent binding of OPs. In particular, C-terminal alpha helices are completely red, opposite from what was found in Fas2*AChE complexes. The magnitude of the C terminal alpha helix motions is much larger for the POX-hAChE conjugate. Consistent exceptions in both structures are expanding positions of Glu and His of the catalytic triad and a small loop around Tyr133, a residue known to protrude into the choline binding site of the active center with hydrogen bonding capacity (8). The clear and significant difference between two covalent conjugates is in the acyl pocket where sharp, blue 1.2 Å positive „ Δ distance” peak is observed at the position 296 of POX-hAChE, combined with smaller, 0.26 Å expansion of the peripheral site Trp286 and opposed by 0.8-0.6 Å contractions at posi-

tions 291 and 292 of the acyl pocket. This severe distortion of the acyl pocket loop specific for the POX-hAChE was well described before (9) and is a consequence of a lack of space in the hAChE acyl pocket for stabilization of phosphorus bound ethoxy substituent in the POX conjugate as opposed to much smaller methyl substituent in the sarin conjugate that fits available acyl pocket space well. In addition, or as a consequence several C-terminal alpha helices move closer to the active serine. Parts of those movements have been already noted (9) but overlay-independent analysis provides a more complete picture of the backbone distortions in the POX-hAChE by indicating compression of an additional alpha helix in positions between 410 and 420. That helix is located immediately below the acyl pocket area and could be in position to serve as a first structural link between the covalently bound OPs and C-terminal helices of the AChE dimeriza-

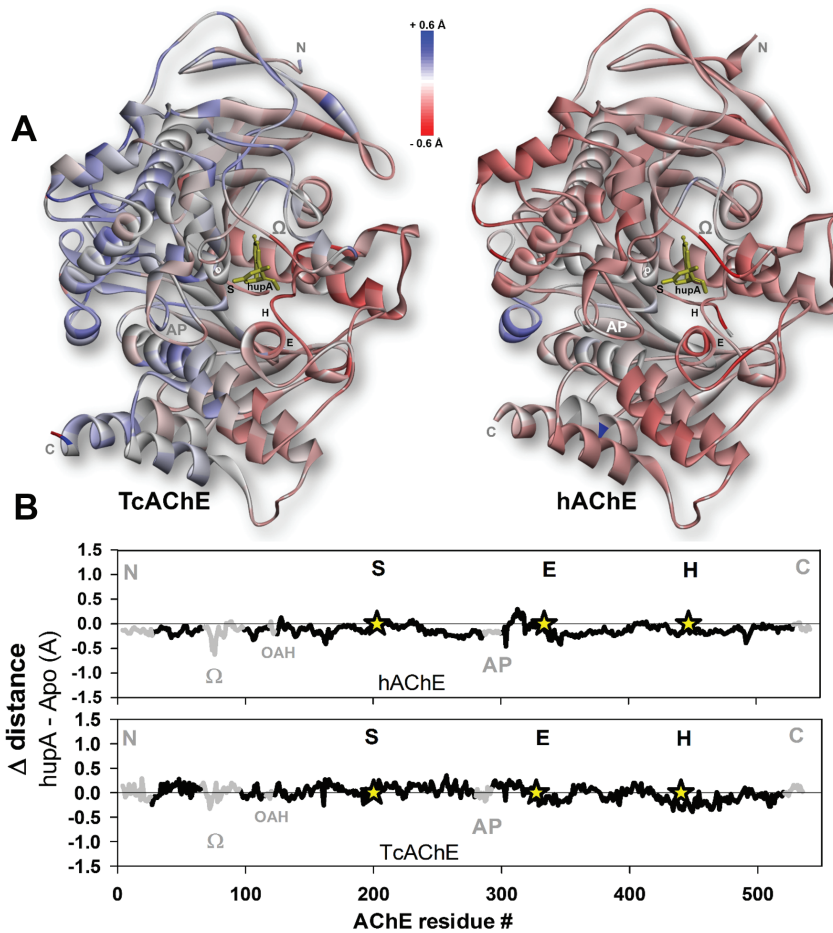


Figure 4. Overlay-independent analysis for the influence of reversible binding of *hupA* on backbone conformations of *TcAChE* (1VOT) and *hAChE* (4EY5). *HupA* is represented by yellow sticks. Positions of catalytic triad residues (S,E,H: residues Ser200, Glu327, His440 in *TcAChE* and Ser203, Glu334, His447 in *hAChE*), oxyanion hole (OAH: residues 117-119 in *TcAChE* and 120-122 in *hAChE*), Ω loop (residues 67-94 in *TcAChE* and 69-96 in *hAChE*) and acyl pocket loop (AP: residues 281-291 in *TcAChE* and 288-298 in *hAChE*) are indicated both in structures (A) and in graphs (B) as described in the Fig 1 legend.

tion domain. In the linear AChE sequence this helix is located between Glu334 and His447 of the catalytic triad and represents one of two most significant contraction area peaks in both OP conjugates. The same helix was pushed away from the active serine in Fas2*AChE complexes as described above. We are thus identifying a structural element of the AChE backbone with capacity to change its conformation depending on the nature of a ligand bound to AChE. Conformational flexibility of the same helix was also observed in sarin and tabun conjugated mAChE (data not shown).

Recently the first high yield bacterial expression of a correctly folded, catalytically functional AChE was achieved (10). The 51 simultaneous mutations created by automated protein sequence design were necessary, resulting in expression of a non-glycosylated hAChE mutant (10). The readily determined X-ray 3D structure of this mutant allows for analysis on degree of structural similarity of its backbone fold with unliganded (Apo) wt hAChE

and nature of driving forces that led to „self-stabilization” of this protein during its expression in bacteria, even in the absence of N-linked polysaccharide chains. Overlay-independent analysis reveals (Figure 6) that positions of most of the mutations (31 out of 51) that resulted in a more stable, easier-to-correctly-fold protein were located in backbone fragments that moved closer to the active serine Ser203.

Apart from general similarity in positions of the functionally important structural elements in the mutant that include catalytic triad, the oxyanion hole, Ω loop and acyl pocket loop, conformation of the mutant backbone shows few sharp peaks of difference (Figure 6B) but only in the flexible surface loops. Two of the C-terminal alpha helices observed to contract in OP conjugated hAChE, showed contraction in this structure, as well, as a possible consequence of covalently bound VX to the active center serine.

In the above analyzed structures of POX-hAChE conjugate and Fas2*AChE complexes overlay-independent

Table 1. Influences of reversible complex formation, covalent conjugate formation or extensive mutagenesis on hAChE quaternary structure in the crystal. Angles between monomer normal vectors calculated for three planes using eq. 6 were subtracted from angles determined for nonliganded, wt AChE (4EY4; Apo) to yield “ Δ Angle” values indicative of quaternary structure change.

hAChE structure	PDB ID	Space group	Cell dimensions	Δ Angle (deg)		
				X-Y plane	Y-Z plane	X-Z plane
Apo	4EY4	P 3 ₁ 2 1	106.18 x 106.18 x 324.4	0.0	0.0	0.0
Donepezil complex	4EY7	P 3 ₁ 2 1	105.15 x 105.15 x 322.9	-0.065	-0.12	-0.069
POX-conjugate	5HF5	P 3 ₁ 2 1	104.92 x 104.92 x 322.8	0.98	1.3	2.5
51-x mut VX-conjugate	5HQ3	P 4 ₃ 2 ₁ 2	89.53 x 89.53 x 395.3	-0.91	-3.3	-7.2
Fas2 complex	4EY8	H 3 2	151.71 x 151.71 x 247.86	0.96	-2.3	-6.5

analysis revealed possible correlation between ligand binding and AChE backbone movements in the C-terminal alpha helices that form dimerization AChE domain. Fas2 tight binding caused them to expand and covalent conjugation of the active serine to contract towards the active serine. Since modifications at the dimerization in-

terface could affect quaternary structures of hAChE homodimers, we analyzed relative positions of monomers in crystallographic hAChE dimers formed by apo hAChE, Fas* hAChE complex, POX-hAChE conjugate, donepezil* hAChE complex, sarin-hAChE conjugate and VX-51-x hAChE mutant. The RMSD overlay of dimers

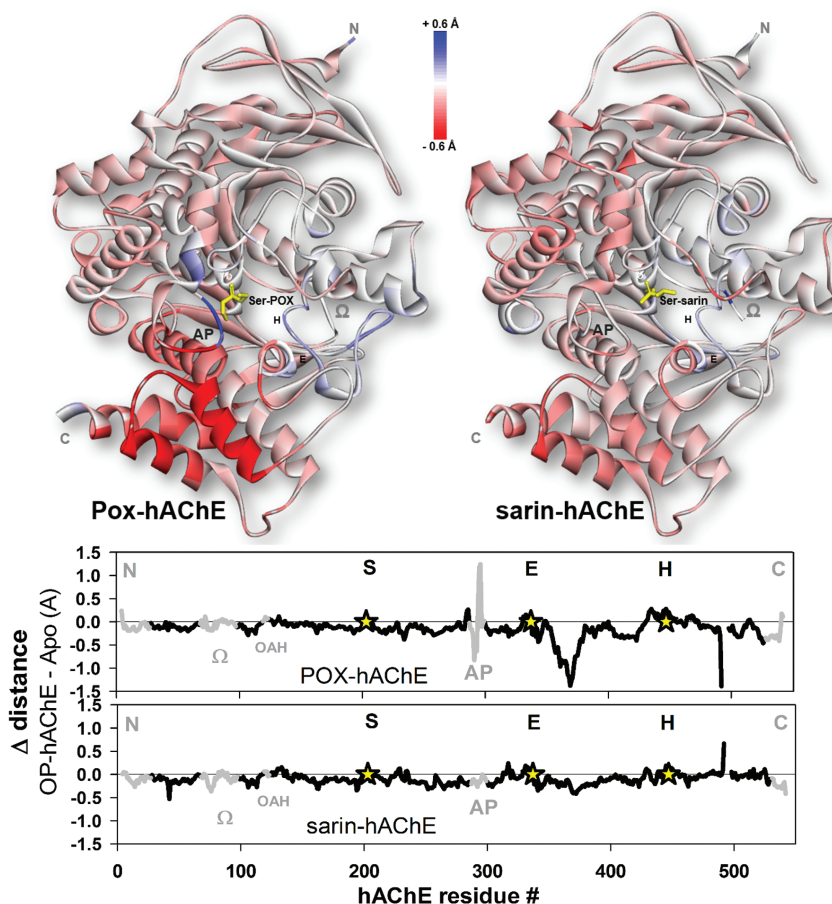


Figure 5. Overlay-independent analysis of the influence of covalent conjugation of hAChE by OPs paraoxon (POX; 5HF5) and sarin (5FPQ), on the backbone conformation of hAChE. Conjugated OPs are shown as yellow sticks. Positions of catalytic triad residues (S,E,H; residues Ser203, Glu334, His447), oxyanion hole (OAH; residues 120-122), Ω loop (residues 69-96) and acyl pocket loop (AP; residues 288-298) are indicated both in structures (A) and in graphs (B) as described in the Fig 1 legend.

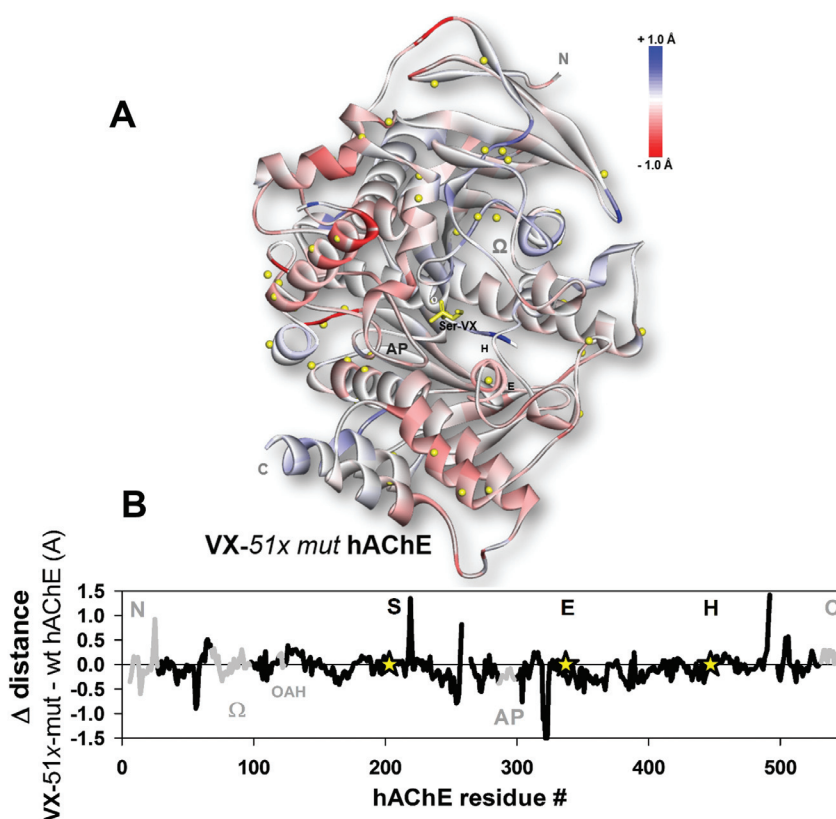


Figure 6. Overlay-independent analysis of the influence of simultaneous 51 site-directed mutations on the backbone conformation of VX conjugated hAChE (5HQ3). Positions of alpha carbons of mutated residues are shown as yellow spheres. Positions of catalytic triad residues (S,E,H: residues Ser203, Glu334, His447), oxyanion hole (OAH: residues 120–122), Ω loop (residues 69–96) and acyl pocket loop (AP: residues 288–298) are indicated both in the structure (A) and in the graph (B) as described in the Fig 1 legend. VX in the structure is shown as yellow sticks.

where only one of monomers was used for the overlay revealed systematic deviations in position of the other monomer, from the position found in apo hAChE, for Fas2* hAChE complex, POX-hAChE conjugate and VX-51-x hAChE mutant (Figure 6, Table 1). A very small shift was observed for sarin-hAChE conjugate (data not shown) and no shift for donepezil* hAChE complex. An overlay-independent analysis of homodimeric quaternary structures revealed spatially similar monomer tilts in dimers of the Fas2* hAChE complex and VX-51-x hAChE mutant, while tilt of the POX-hAChE conjugate was differently oriented (Figure 6; Table 1). This was revealed in both „Δ distance” graphs and „Δ angle” values. It seems obvious that conformational modifications in the tertiary structure of the Fas2* hAChE complex at the C-terminus extended to the second monomer of the homodimer influencing its relative orientation and overall quaternary structure. It appears less clear, however, how 51 mutations in combination with VX conjugation resulted in very similar quaternary structure change (Figure 6), in the absence of clear similarity in tertiary structure modifications (Figures 2 and 5) and absence of significant conformational changes of the VX-51-x hAChE mutant at the dimerization interface. Nevertheless, the absence of sur-

face N-linked polysaccharide chains in the mutant could have been sufficient enough for relative orientations of dimers to change, compared to apo wt hAChE. It is fascinating that reversible, tight binding of Fas2 to hAChE appears to result in a similar kind of protein stabilization as 51-fold mutations, combined with VX conjugation and the absence of glycosylation.

CONCLUSIONS

Application of the overlay-independent analysis to a variety of AChE X-ray 3D structures reveals that in spite of high similarity in their monomeric alpha carbon folds, reflected in low overlay RMSD values, ligand binding associated systematic conformational changes of AChE backbone routinely occur. Although typically sub angstrom to angstrom in magnitude they can lead to alterations in crystallographic quaternary structures and are illustrative of kind of motions that are larger in magnitude and likely occur at physiological temperatures and in solution. In spite of relatively small magnitudes that compared to X-ray structure resolutions may seem insignificant, the fact that they refer to commonly well-defined backbone positions and that they systematically occur in discrete

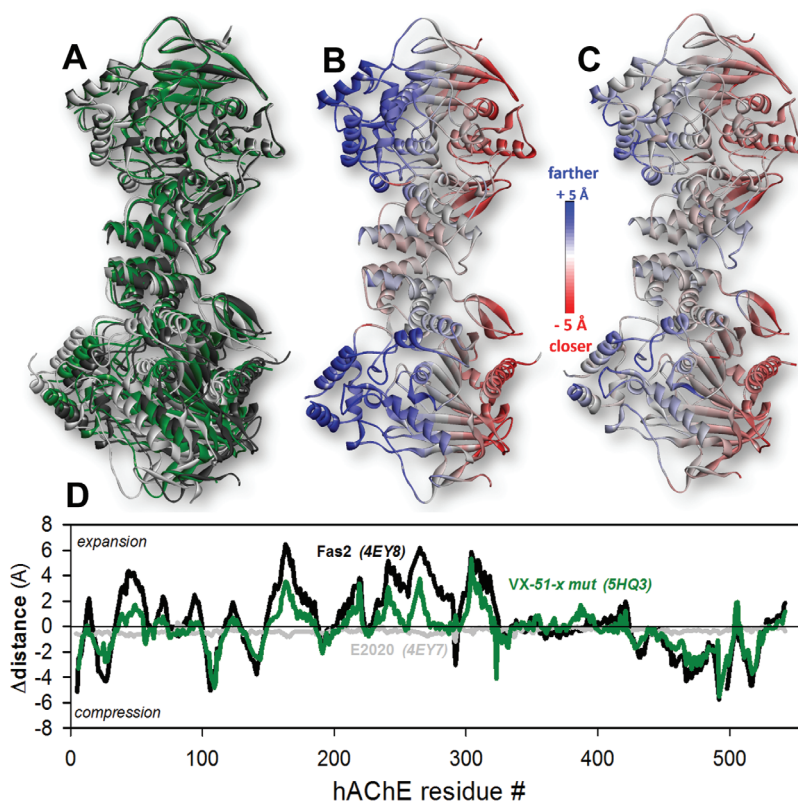


Figure 7. Quaternary structure alterations in dimers of human AChE influenced by reversible Fas2 binding and by simultaneous 51-fold site directed mutagenesis combined with covalent conjugation by VX. **A)** RMSD based overlay of hAChE dimers using only one monomer as a template (apo hAChE, 4EY4, shown as a light-grey ribbon) with Fas2 complex (4EY8, shown as a black ribbon) and 51-fold mutant (5HQ3; shown as a green ribbon). **B)** Overlay-independent analysis of the influence of reversible, tight Fas2 binding and **C)** analogous analysis of simultaneous 51 site-directed mutations on the hAChE dimer **D)** Graphs of “ Δ distances” determined between alpha carbons of equivalent residues in two different monomers, compared to distances determined for the apo hAChE (4EY4). Donepezil complex with hAChE (E2020; 4EY7, grey graph trace) showed no difference in monomer position compared to the Apo wt hAChE.

structural domains, even in structures of analogous proteins from different species provide necessary justification for their significance and usefulness of the approach. We demonstrated here that structurally diverse ligands leading to different mechanisms of interactions with AChEs result in specific local alterations in its backbone fold. Tight binding surface inhibitor Fas2 causes global expansion of AChE structures except for areas of immediate contact. Covalent OP inhibitors largely cause structure to compress, similar as nM affinity active center inhibitor hupA. We observe here previously unnoted influence of acyl pocket interacting ligands, including both covalent inhibitors and Fas2, on conformational flexibility of C-terminal alpha helices at the dimerization interface that can lead to alterations in the crystallographic AChE quaternary structure. The observed magnitudes of quaternary structure movements of up to $\pm 8 \text{ \AA}$ further confirm value and reliability of overlay-independent tertiary structure analyses that are capable of detecting small backbone shifts subsequently amplified into more notable quaternary structure modifications.

ACKNOWLEDGEMENTS

This research was supported by the CounterACT Program, National Institutes of Health Office of the Director (NIH OD), and the National Institute of Neurological Disorders and Stroke (NINDS), Grant Numbers U01NS083451 and R21NS098998.

REFERENCES

- Schumacher M, Camp S, Maulet Y, Newton M, MacPhee-Quigley K, Taylor SS, Friedmann T, Taylor P. 1986 Primary structure of *Torpedo californica* acetylcholinesterase deduced from its cDNA sequence. *Nature*. 319: 407-409. <https://doi.org/10.1038/319407a0>
- MacPhee-Quigley K, Vedvick TS, Taylor P, Taylor SS. 1986 Profile of the disulfide bonds in acetylcholinesterase. *J Biol Chem*. 261:13565-13570.
- Sussman JL, Harel M, Frolow F, Oefner C, Goldman A, Toker L, Silman I. 1991 Atomic structure of acetylcholinesterase from *Torpedo californica*: a prototypic acetylcholine-binding protein. *Science*. 253: 872-879. <https://doi.org/10.1126/science.1678899>
- Radić, Z., Taylor, P. 2006 Structure and Function of Cholinesterases. In: Gupta, R., (editor) *Toxicology of Organophosphate and*

- Carbamate Compounds, Elsevier, Amsterdam, p.161-186.
<https://doi.org/10.1016/B978-012088523-7/50013-2>
5. Kovalevsky A, Blumenthal DK, Cheng X, Taylor P, Radić Z. 2016 Limitations in current acetylcholinesterase structure-based design of oxime antidotes for organophosphate poisoning. *Ann N Y Acad Sci.* 1378: 41-49. <https://doi.org/10.1111/nyas.13128>
 6. Harel M, Kleywegt GJ, Ravelli RB, Silman I, Sussman JL. 1995 Crystal structure of an acetylcholinesterase-fasciculin complex: interaction of a three-fingered toxin from snake venom with its target. *Structure.* 3: 1355-1366.
[https://doi.org/10.1016/S0969-2126\(01\)00273-8](https://doi.org/10.1016/S0969-2126(01)00273-8)
 7. Radić Z, Taylor P. 2001 Interaction kinetics of reversible inhibitors and substrates with acetylcholinesterase and its fasciculin 2 complex. *J Biol Chem.* 276: 4622-4633.
<https://doi.org/10.1074/jbc.M006855200>
 8. Ordentlich A, Barak D, Kronman C, Ariel N, Segall Y, Velan B, Shafferman A. 1995 Contribution of aromatic moieties of tyrosine 133 and of the anionic subsite tryptophan 86 to catalytic efficiency and allosteric modulation of acetylcholinesterase. *J Biol Chem.* 270: 2082-2091. <https://doi.org/10.1074/jbc.270.5.2082>
 9. Franklin MC, Rudolph MJ, Ginter C, Cassidy MS, Cheung J. 2016 Structures of paraoxon-inhibited human acetylcholinesterase reveal perturbations of the acyl loop and the dimer interface. *Proteins.* 84:1246-1256. <https://doi.org/10.1002/prot.25073>
 10. Goldenzweig A, Goldsmith M, Hill SE, Gertman O, Laurino P, Ashani Y, Dym O, Unger T, Albeck S, Prilusky J, Lieberman RL, Aharoni A, Silman I, Sussman JL, Tawfik DS, Fleishman SJ. 2016 Automated Structure- and Sequence-Based Design of Proteins for High Bacterial Expression and Stability. *Mol Cell.* 63: 337-346.
<https://doi.org/10.1016/j.molcel.2016.06.012>